Biophysical Journal, Volume *117*

Supplemental Information

Dynamics of the *E. coli* β-Clamp Dimer Interface and Its Influence on DNA Loading

Bilyana N. Koleva, Hatice Gokcan, Alessandro A. Rizzo, Socheata Lim, Kevin Jeanne Dit Fouque, Angelina Choy, Melissa L. Liriano, Francisco Fernandez-Lima, Dmitry M. Korzhnev, G. Andrés Cisneros, and Penny J. Beuning

Supporting Methods and Results

Protein Expression and Purification

For most experiments, *E. coli* BL21(DE3) was transformed with pET11T expressing WT β or β clamp variants. Transformants were selected on Luria-Bertani (LB) plates supplemented with ampicillin. A 50-mL starter culture in a shake flask (200 rpm) was grown overnight at 37 °C. A 1-L culture was seeded for each protein and grown at 37 °C until an optical density (OD) at 600 nm of 1.0 was reached. Protein expression was induced with isopropyl β-D-1-thiogalactopyranoside (IPTG) to a final concentration of 1 mM at 22 °C for 16-18 h. Cells were harvested by centrifugation for 10 min at 6,750 × g at 4 °C and frozen at -80 °C or lysed immediately. Protein overexpression was confirmed using sodium dodecyl sulfate-polyacrylamide gel electrophoresis (SDS-PAGE).

Cell pellets for β clamp purification were resuspended on ice in 20 mM HEPES, pH 7.5, 100 mM NaCl, 0.1 mM EDTA, 2 mM DTT, 10% glycerol (Buffer A) supplemented with 10 μg/mL phenylmethanesulfonyl fluoride (PMSF), and cOmplete^{TM} mini protease inhibitor cocktail (Roche, Sigma, St. Louis, MO). Cells were lysed by sonication and cell debris was pelleted by centrifugation at 14,000 × g at 4 °C for 1 h. The lysate was loaded onto a 2 × 5 mL HiTrap DEAE FF (GE Healthcare) column and eluted with Buffer A and increasing NaCl concentration to 1 M. Pooled fractions were diluted 1:1 in a buffer containing 20 mM HEPES, pH 7.5, 0.1 mM EDTA, 2 mM DTT, 10% glycerol, and 1 M ammonium sulfate, loaded onto 2 × 5 mL HiTrap Phenyl FF high sub (GE Healthcare), and eluted in a buffer with the same composition except ammonium sulfate was omitted. Pooled fractions were concentrated using VivaSpin 20, 10,000 Da MWCO concentrators (Sartorius, Cambridge, MA) and loaded onto Superdex 75 (GE Healthcare). Proteins were stored in 20 mM HEPES, pH 7.5, 50 mM NaCl, 0.1 mM EDTA, 1 mM DTT, and 10% glycerol at -80 °C for subsequent analysis. Protein concentration was measured using the Bradford assay with bovine serum albumin (BSA) as a reference (Sigma). Final purity was assessed using SDS-PAGE.

For ITC, *E. coli* BL21(DE3) was transformed with plasmids encoding corresponding proteins and grown to mid-log phase at 37 °C in LB media containing 50 μg/mL kanamycin. Protein expression was induced by 1 mM IPTG at 20 °C overnight. Cells were harvested and lysed by sonication. The lysate was centrifuged and filtered, followed by protein purification on a Talon Co^{2+} affinity column (Clontech, Mountain View, CA). The His-tag was cleaved with thrombin and a final purification step was performed on HiLoad Superdex-75 (mini-δ) or Superdex-200 (β clamp) size-exclusion columns (GE Healthcare). The purified mini-δ and β clamp variants were concentrated to 0.6-0.7 mM and 0.1 mM, respectively, and dialyzed into a buffer containing 100 mM sodium phosphate, 100 mM NaCl, 500 μM β-mercaptoethanol (βME), pH 7.4. Prior to ITC studies, protein samples were cleared by centrifugation at 14,000 rpm for 30 min and degassed for at least 30 min.

ATPase assay

The assay was performed as per the BIOMOL® Green manual (Enzo Life Sciences). To anneal DNA, equimolar amounts of 5'-biotinylated primer (5′-Biotin-AGTTCTTCTGCAATAACTGGCCGT CGTTTGAAGATTTCG-3′, IDT, Coralville, IA) and 5′-biotinylated template (5′-biotin-CCATTCTGT AACGCCAGGGTTTTCGCAGTCAACATTCGAAATCTTCAAACGACGGCCAGTTATTGC-3′) were combined in STE buffer (10 mM Tris-HCl, pH 8.0, 50 mM NaCl, 0.1 mM EDTA). Annealing reactions were incubated at 95 °C for 2 min, 50 °C for 30 min, and slowly cooled to room temperature. Assay samples were prepared in 100 μL reactions containing 50 pmol β_2, 50 pmol γ complex, 50 pmol annealed dsDNA, and 1 mM ATP in 1x ATPase assay buffer (30 mM HEPES, pH 7.5, 1 mM DTT, 7 mM $MgCl_2$).

Reactions were incubated for 5 min at 37 °C, following which 1 mL of BIOMOL® Green reagent was added to each sample and incubated for an additional 20 min at 22 °C. Samples (1 mL) were then transferred to a cuvette and OD_{620} was measured. For quantitation, a standard curve was prepared using inorganic phosphate. The linear range of the assay in the cuvette format is from 0.5 nmol to 16 nmol of phosphate released. Each reaction was assembled in triplicate. Average nmol of phosphate released and standard deviations are reported.

Clamp loading assay

To anneal DNA, equimolar amounts of 5′-biotinylated primer (5′-AGTTCTTCTGC AATAACTGGCCGTCGTTTGAAGATTTCG-3′) and template (5′-ACGACCGTCCCATTCTGTAACG CCAGGGTTTTCGCAGTCAACATTCGAAATCTTCAAACGACGGCCAGTTATTGC-3′) were added in STE buffer (10 mM Tris-HCl, pH 8.0, 50 mM NaCl, 0.1 mM EDTA). Annealing reactions were incubated at 95 °C for 2 min, 50 °C for 30 min, and slowly cooled to room temperature. Streptavidin magnetic beads (New England Biolabs) were washed with 1x B/W buffer (5 mM Tris-HCl, pH 7.5, 0.5 mM EDTA, 1 M NaCl) three times to remove storage solution. For the bioconjugation, 200 pmol of biotinylated dsDNA was combined with 1 mg of streptavidin beads in 40 µL in 1x B/W buffer. Binding was achieved by incubation at 22 °C for 1 h on a rotator. The beads were washed two times in 1x B/W buffer to remove unbound DNA and two more times in 1x loading assay buffer (30 mM HEPES, pH 7.5, 7 mM $MgSO_4$, 1 mM DTT, 1 mM CHAPS). Loading reactions were performed by resuspending the bead-DNA conjugate in 25 µL 1x loading assay buffer containing 200 pmol β_2, 200 pmol γ complex, 1 mM ATP, and 5 µg SSB. After 5 min incubation at 37 °C, 5 µL bead resuspension was applied to the magnet, with the unloaded β in the supernatant and the loaded β in the pellet fraction. The beads were washed three times in 1x loading assay buffer by tapping gently to remove unbound proteins. At indicated time points (0, 60 min), 10 µL bead resuspension was removed from the reaction and applied to the magnet to probe for loaded vs. unloaded β. The reactions were incubated at 22 °C on a rotator while collecting the time points. Loading controls were assembled separately to show the amount of β in reactions. All samples were normalized based on the quantified amount of protein in the loading control and incubated in 1x SDS loading buffer (62.5 mM Tris-HCl, pH 6.8, 0.01% Bromophenol Blue, 2.5% βME, 10% glycerol, 2% SDS) for 10 min at 95 °C prior to resolution by 12% SDS-PAGE. Assays were carried out with loading amounts within the linear range of quantitation, or if samples were diluted prior to loading in order to remain within the linear range, this dilution factor was accounted for in the calculations of the amount of β in each fraction. Electrophoresed proteins were transferred to polyvinylidene difluoride (PVDF) membrane in 10 mM CAPS, pH 10.0, 10% methanol buffer. Gels were stained with Coomassie gel stain after transfer to ensure proteins were transferred. Membranes were blocked overnight in 2.5% milk/2.5% BSA in 20 mM Tris-HCl, pH 7.6, 137 mM NaCl, 0.1% Tween-20 (TBS-T). Membranes were incubated with rabbit anti-β primary antibody and goat anti-rabbit Alexa-647 (Thermo Fisher) secondary antibody for 1 h each at 22 °C in 2.5% milk/2.5% BSA TBS-T buffer. Membranes were washed three times, 5 min each in TBS-T buffer after each antibody incubation. Proteins were detected on a Storm 860 phosphorimager using excitation at 635 nm and analyzed using ImageQuant TL 1D Gel Analysis software (GE Healthcare). Loading assays were repeated three times and the average amount of loaded/unloaded β and the standard deviations are reported.

Immunoblotting

Wild-type β and variants of the β clamp were expressed in MS120 cells at the non-permissive growth temperature 37 °C. Expression was induced with 0.5 mM IPTG in LB for 18 h. The OD_{600} was measured and used to normalize the volume of cells to be collected for each variant. Centrifugation was used to harvest cells that were then resuspended in 300 µL 0.85% saline and 100 µL 4X SDS-dye. Samples were

heated to 95 °C for 30 min to lyse the cells and denature the proteins. Proteins were resolved by 16% SDS-PAGE and transferred to polyvinylidene difluoride (PVDF) membranes at 4 °C and processed as above. Membranes were then imaged on an iBright (Invitrogen) on the Alex-fluor 647 channel.

Molecular Dynamics Results

Effect of the mutations on atomic fluctuations. Nine residues with a change in relative RMSF value greater than ±1 Å were observed for the different variants (Fig. S11). P20′, L21′, and G22′ on Monomer B become more mobile in the L82E variant (Fig. S11, *green*) relative to WT β. D120′, which is located on the inter-domain connector loop (IDCL) between Domain 1 and Domain 2, becomes more mobile in the S107R variant (Fig. S11, *cyan*), while the mobility of D120′ is observed to be either very similar to that of the WT protein or calculated to be less than that of WT β for all other variants. The mobility of G209, G210, and D211 are affected by different mutations, where the highest increase is seen for the T45R variant (Fig. S11, *yellow*). The same region on Monomer B (G209′, G210′, and D211′) becomes less mobile in the context of almost all of the mutations except for the T47R variant (Fig. S11, *magenta*). L248, which is in close proximity to the hydrophobic pocket where β-interacting proteins bind (residues 247, 360, 363) (19, 57, 89), becomes more mobile on Monomer A in the β L82E I272A variant (Fig. S11, *blue*). Similar results are seen for the residue K250, located on the IDCL between Domain 2 and Domain 3.

Cross correlation in the dimer interface. Helix-3 (H3) and Helix-21 (H21) are observed to be mostly positively correlated in the L82E, T45R, and S107R variants (Fig. S12A, region colors: *blue-cyan*) while negative correlations are found for the remaining systems relative to WT β. Most of the residues on H3 and Sheet-5A (S5A) are computed as negatively correlated in the L82D variant (Fig. S12A, region colors: *blue-yellow*) while H3 and Sheet-6A (S6A) are found positively correlated in the T45R variant (Fig. S12A, region colors: *blue-orange*). The L82D variant results in anti-correlation between the tail residues of Sheet-3A (S3A) and H21 unlike in other systems (Fig. S12A, region colors: *red-cyan*). A similar result is found for the correlation between the head residues of Sheet-4A (S4A) and tail residues of H21 in the L82D variant (Fig. S12A, region colors: *green-cyan*). The β L82E variant also exhibited increased correlation between the tail residues of S4A and H21 (Fig. S12A, region colors: *green-cyan*), while the additional I272A mutation in the L82E I272A variant results in the highest S4A-H21 correlations.

In the case of the second domain interface between Domain 3 and Domain 1′, Helix-10 (H10) and Helix-14 (H14) are observed to be correlated in the T45R and S107R variants (Fig. S12B, region colors: *blue-cyan*). Almost all the residues on H10 are positively correlated with Sheet-5D (S5D) (Fig. S12B, region colors: *blue-yellow*) and Sheet-6D (S6D) (Fig. S12B, region colors: *blue-orange*) in the T45R variant. Almost all residues on H14 are negatively correlated with Sheet-3D (S3D) and Sheet-4D in the L82E variant but the additional I272A and I272′A mutations in the L82E I272A variant result in positive correlations between H14 and S4D in this variant.

The mutations in the L82E and L82E I272A variants increase the number of residues in β sheets that are correlated with each other on the domain interface between Domain 1 and Domain 3′. The region composed of residues from L82 to R96 in particular is found to be highly correlated with the region composed of residues Y282′ to N295′ in these variants. It is noteworthy that the magnitude of the correlations between these β sheets is the highest in the L82E I272A variant relative to the other systems. The loops comprising residues 82-86 and 274′-279′ in the L82D variant have the highest anti-correlation for the Domain 1:Domain 3′ interface (Fig. S12A). For the complementary interface Domain 3:Domain 1′, the corresponding loops (82′-86′ and 274-279) show the highest negative correlations with each other in the L82E variant (Fig. S12B). The loop containing residues 274-279 forms one of the interaction sites with δ (57). In general, the largest perturbations relative to WT β are found in the β L82D, L82E, and L82E I272A variants.

REFERENCES

19. Dalrymple, B.P., K. Kongsuwan, G. Wijffels, N.E. Dixon, and P.A. Jennings 2001. A universal protein-protein interaction motif in the eubacterial DNA replication and repair systems. *Proc Natl Acad Sci U S A*. 98:11627-11632.

57. Jeruzalmi, D., O. Yurieva, Y. Zhao, M. Young, J. Stewart, M. Hingorani, M. O'Donnell, and J. Kuriyan 2001. Mechanism of processivity clamp opening by the delta subunit wrench of the clamp loader complex of *E. coli* DNA polymerase III. *Cell*. 106:417-428.

89. Kelch, B.A., D.L. Makino, M. O'Donnell, and J. Kuriyan 2011. How a DNA polymerase clamp loader opens a sliding clamp. *Science*. 334:1675-1680.

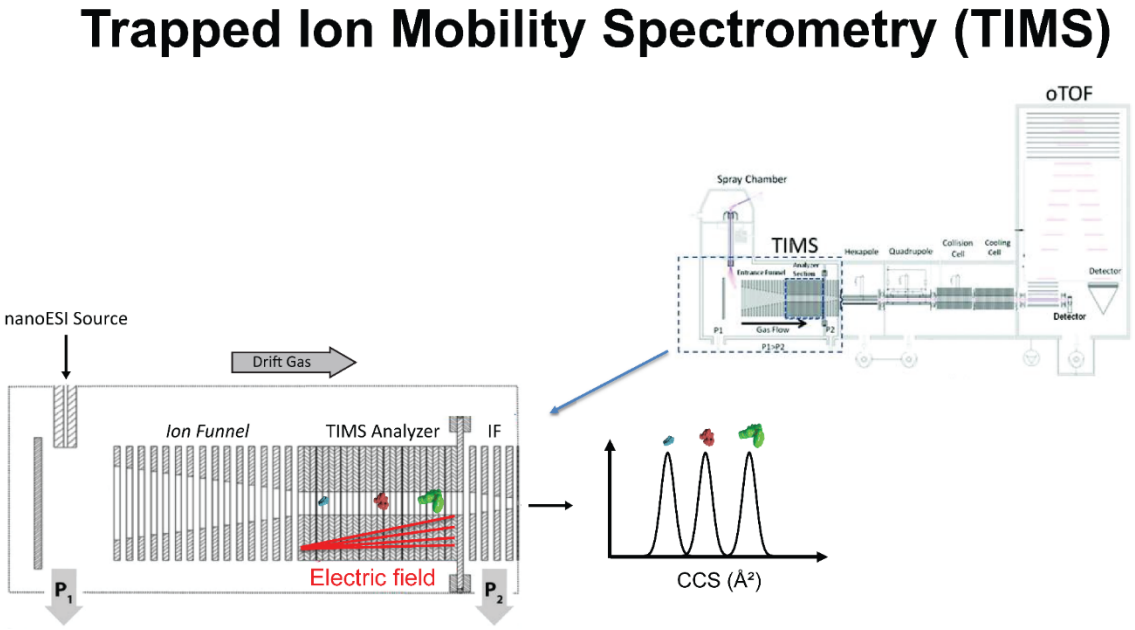

Figure S1. TIMS-MS instrument showing the TIMS cell schematic and TIMS operation.

Table S1. Summary of TIMS experimental ion-neutral collision cross sections (CCS, Å²) and ratios for the multiply protonated species of the *n*-mers clamp variants.

Peptides	CCS (Å²), std. error of mean: ± 0.04%			*n*-mers ratio
	Monomers	Dimers	Tetramers	
Clamp WT	-	**5310** ($[2M+16H]^{16+}$) **5332** ($[2M+17H]^{17+}$) **5325** ($[2M+18H]^{18+}$) **5348** ($[2M+19H]^{19+}$) **5380** ($[2M+20H]^{20+}$)	**7592** ($[4M+25H]^{25+}$) **7682** ($[4M+26H]^{26+}$) **7740** ($[4M+27H]^{27+}$) **7815** ($[4M+28H]^{28+}$)	0/6/1
Clamp L82E	-	**5059** ($[2M+16H]^{16+}$) **5084** ($[2M+17H]^{17+}$) **5129** ($[2M+18H]^{18+}$) **5166** ($[2M+19H]^{19+}$) **5204** ($[2M+20H]^{20+}$)	**7288** ($[4M+24H]^{24+}$) **7341** ($[4M+25H]^{25+}$) **7404** ($[4M+26H]^{26+}$) **7462** ($[4M+27H]^{27+}$) **7537** ($[4M+28H]^{28+}$)	0/3/1
Clamp L82E I272A	**2987** ($[M+10H]^{10+}$) **3066** ($[M+11H]^{11+}$) **3141** ($[M+12H]^{12+}$)	**5063** ($[2M+16H]^{16+}$) **5096** ($[2M+17H]^{17+}$) **5141** ($[2M+18H]^{18+}$) **5173** ($[2M+19H]^{19+}$)	-	1/1/0
Clamp L82D	**2992** ($[M+10H]^{10+}$) **3069** ($[M+11H]^{11+}$) **3144** ($[M+12H]^{12+}$)	-	-	1/0/0

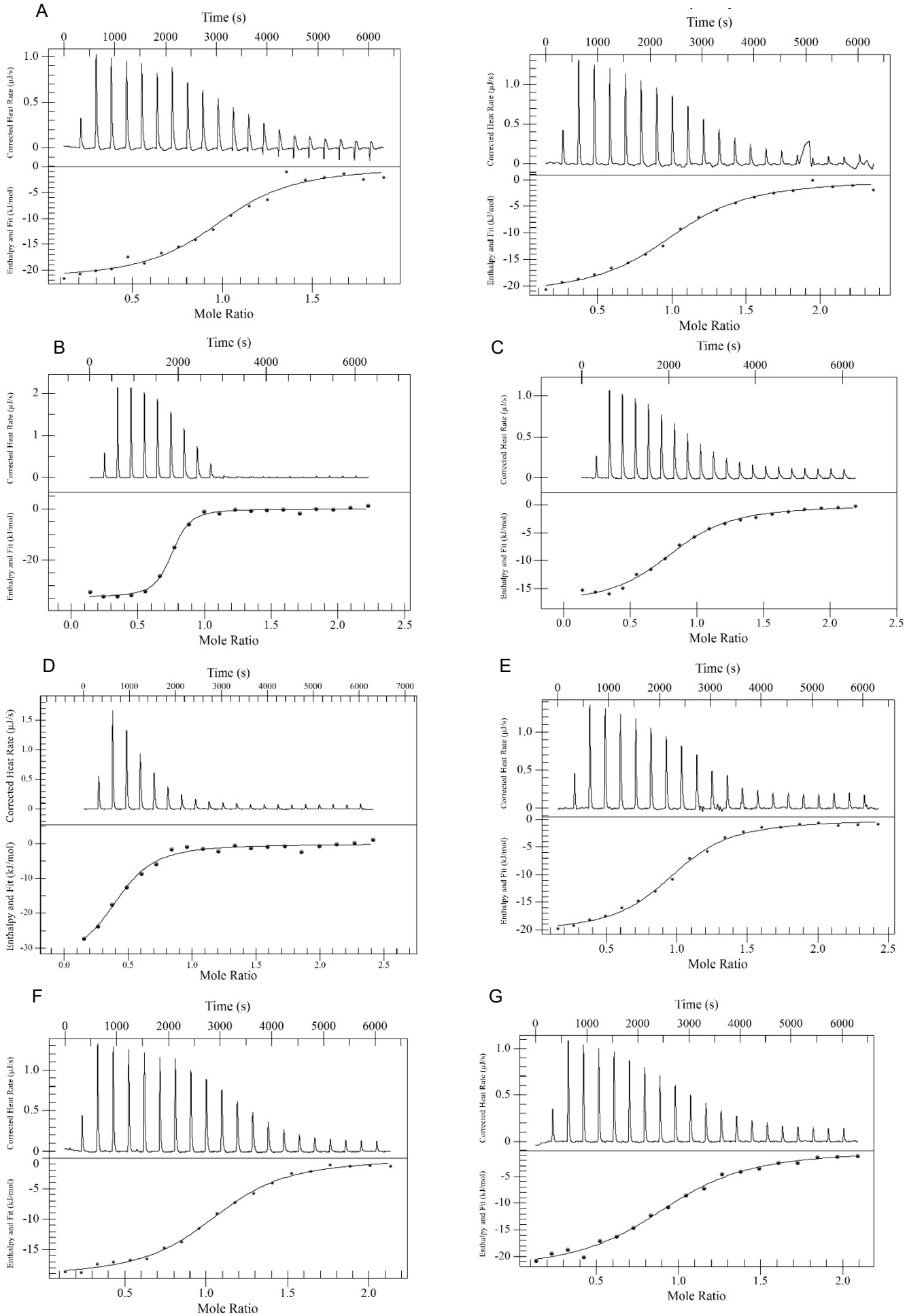
A
Time (s)
Corrected Heat Rate (µJ/s)
Enthalpy and Fit (kJ/mol)
Mole Ratio
B
Time (s)
Corrected Heat Rate (µJ/s)
Enthalpy and Fit (kJ/mol)
Mole Ratio
C
Time (s)
Corrected Heat Rate (µJ/s)
Enthalpy and Fit (kJ/mol)
Mole Ratio
D
Time (s)
Corrected Heat Rate (µJ/s)
Enthalpy and Fit (kJ/mol)
Mole Ratio
E
Time (s)
Corrected Heat Rate (µJ/s)
Enthalpy and Fit (kJ/mol)
Mole Ratio
F
Time (s)
Corrected Heat Rate (µJ/s)
Enthalpy and Fit (kJ/mol)
Mole Ratio
G
Time (s)
Corrected Heat Rate (µJ/s)
Enthalpy and Fit (kJ/mol)
Mole Ratio

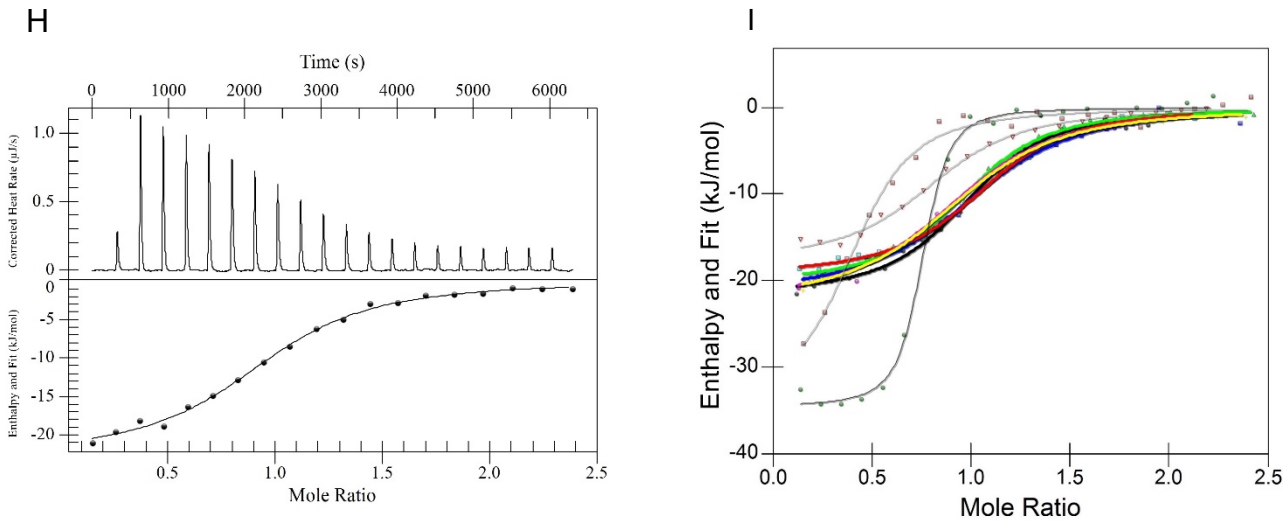

Figure S2. Raw ITC data (top) and integrated heat changes (bottom) obtained during titration into mini-δ solution of the β-clamp variants shown in Table 1: WT (A; 2 replicates), I272A/L273A (B), L82E (C), L82E/I272A (D), S107R (E), S109R (F), T45R (G), T47R (H). (I) Integrated heat changes and their best fits obtained from ITC measurements for mini-δ and β-clamp variants: WT (black, cyan; 2 replicates), I272A L273A (thin black, green circles), S107R (green), S109R (red), T45R (yellow), T47R (magenta), L82E (gray, open triangles), L82E I272A (gray, pink boxes). Thermodynamic parameters are reported in Table 1.

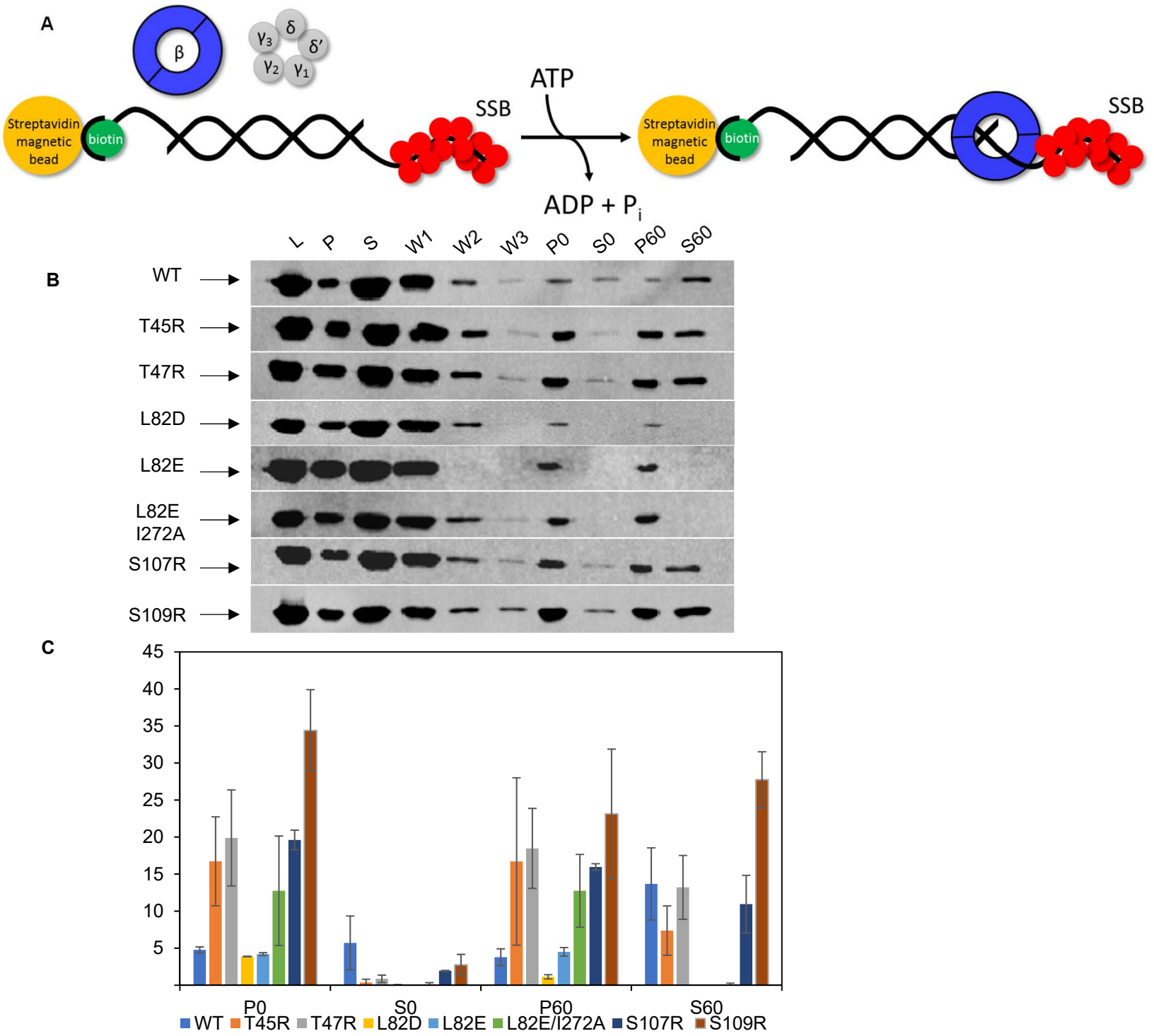

Figure S3. Immunoblot detection of β loaded onto a primer-template substrate using a bead-based assay. (A) Schematic depicting loading of the β clamp onto a primer-template. The biotinylated primer is annealed to a template, resulting in a 3' recessed end. The annealed dsDNA is immobilized on streptavidin magnetic beads. The free 5' end is blocked by SSB (red). Clamp loading reactions are carried out by adding β, γ complex, and ATP to the immobilized DNA at 37 °C. ATP hydrolysis ejects the clamp loader resulting in a stably-loaded clamp. (B) Representative anti-β immunoblots for WT and variant β clamps. Input loading control (L) indicates the amount of β in each loading reaction. Pellet (P) fractions indicate loaded β and supernatant (S) fractions indicate unloaded β. Three consecutive wash steps were performed (shown as W1, W2, and W3). After the wash steps, the pellet and supernatant fractions show the amount of loaded and unloaded β, respectively, for both 0- and 60-min time points. The samples in the first three lanes were diluted 1:4 in order to fit in the linear range of quantitation. In those lanes, the amount loaded/unloaded was multiplied by the dilution factor. (C) Bar graph representing the normalized (based on the input loading control) amount of loaded (pellet) and unloaded (supernatant) β at 0 and 60 min for WT (blue), T45R (orange), T47R (gray), L82D (yellow), L82E (light blue/cyan), L82E I272A (green), S107R (dark blue), and S109R (dark red/brown). Because SSB is present in our reactions and could interact with the β clamp, we investigated whether β interacts with SSB directly by co-expressing and co-purifying both proteins in *E. coli* (Fig. S4).

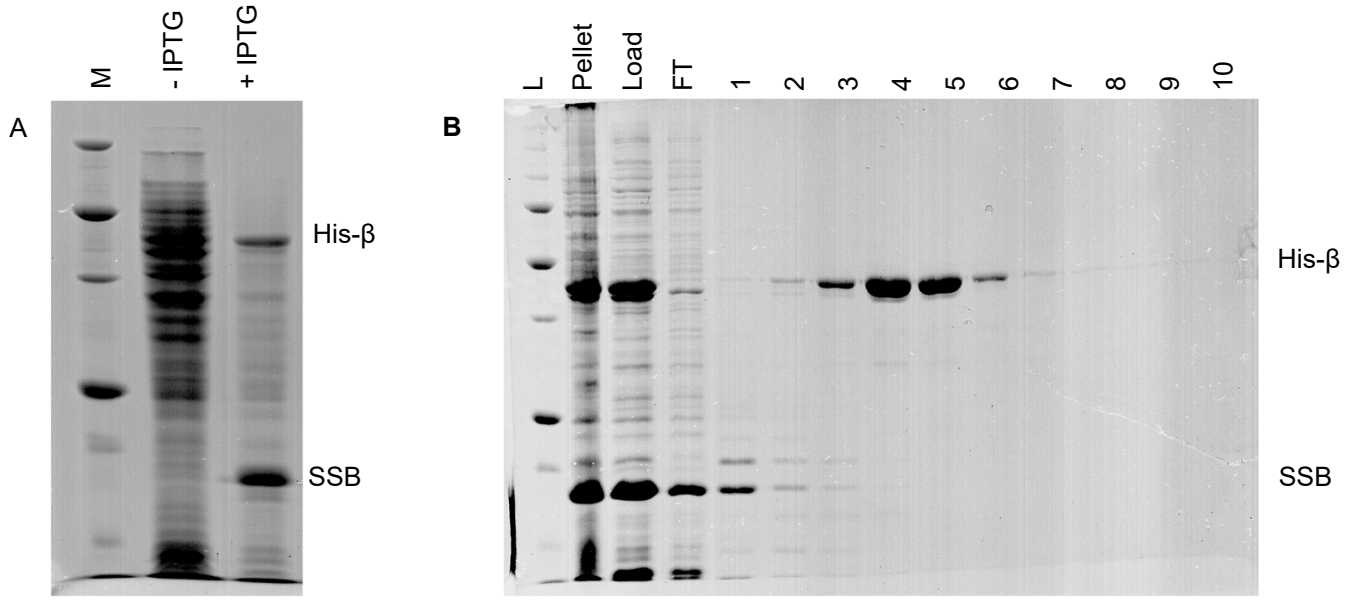

Figure S4. Coexpression to probe for β and SSB interactions. A, Denaturing PAGE showing coexpression of wild-type β (His-tagged) and SSB (untagged). B, Denaturing PAGE demonstrating through Ni^{2+}-affinity chromatography that β and SSB do not coelute. Lysis conditions in the presence and absence of added DNA, additional wash steps and extended gradients were used but it did not appear that β and SSB coelute.

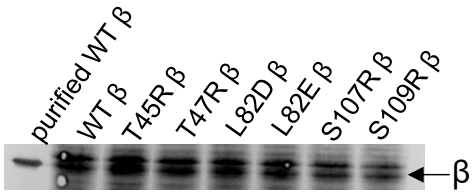

Figure S5. Immunoblot showing expression of WT β and β variants in the MS120 strain at the non-permissive temperature 37 °C. Purified WT β is included as a control. Variants are indicated above the lanes. The L82E I272A does not support growth at 37 °C and therefore was not analyzed.

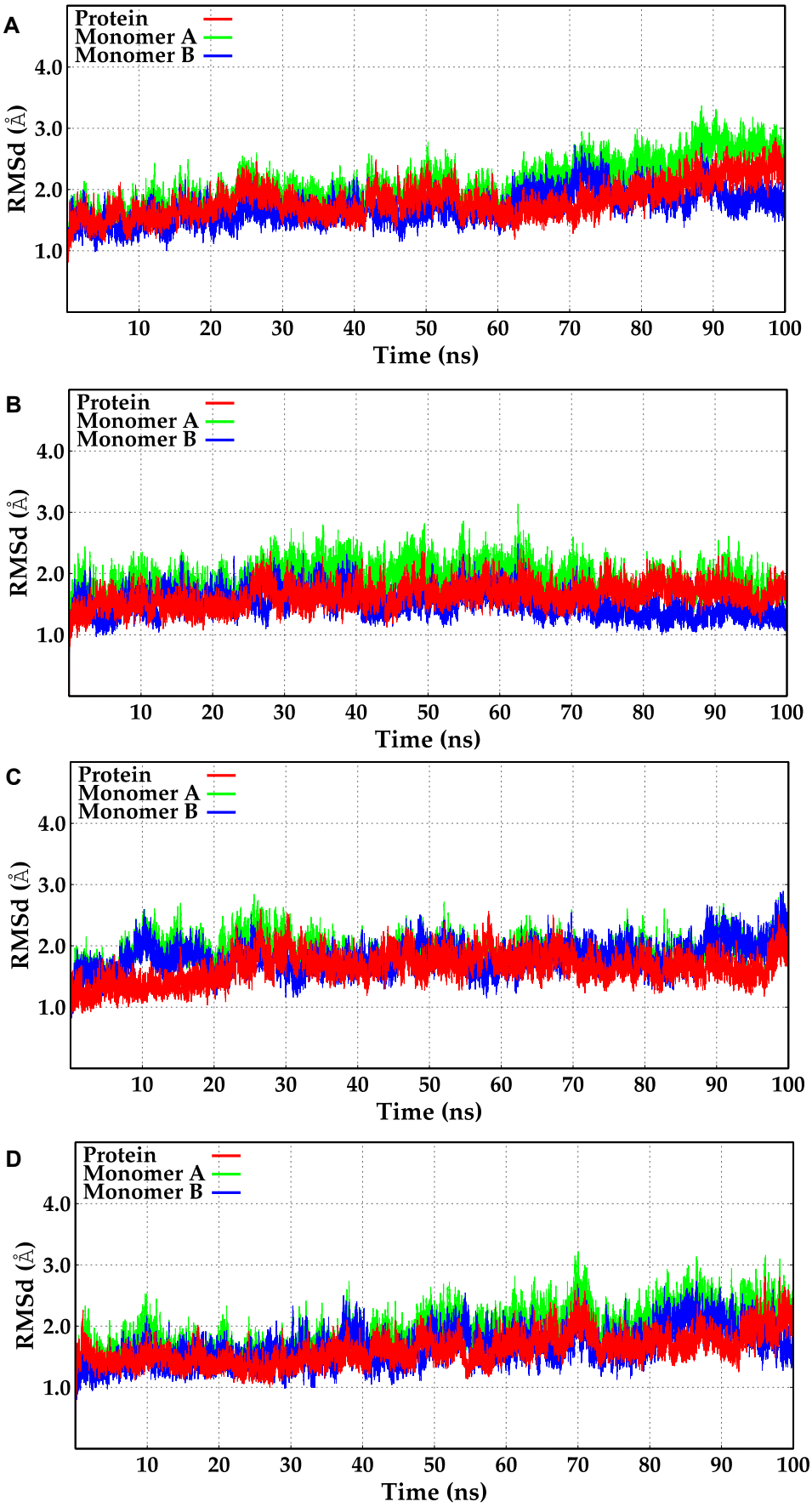

Figure S6. RMSd of backbone atoms (C,C_α,N) along the simulation of (A) WT protein, (B) L82D variant, (C) L82E variant, and (D) L82E I272A variant.

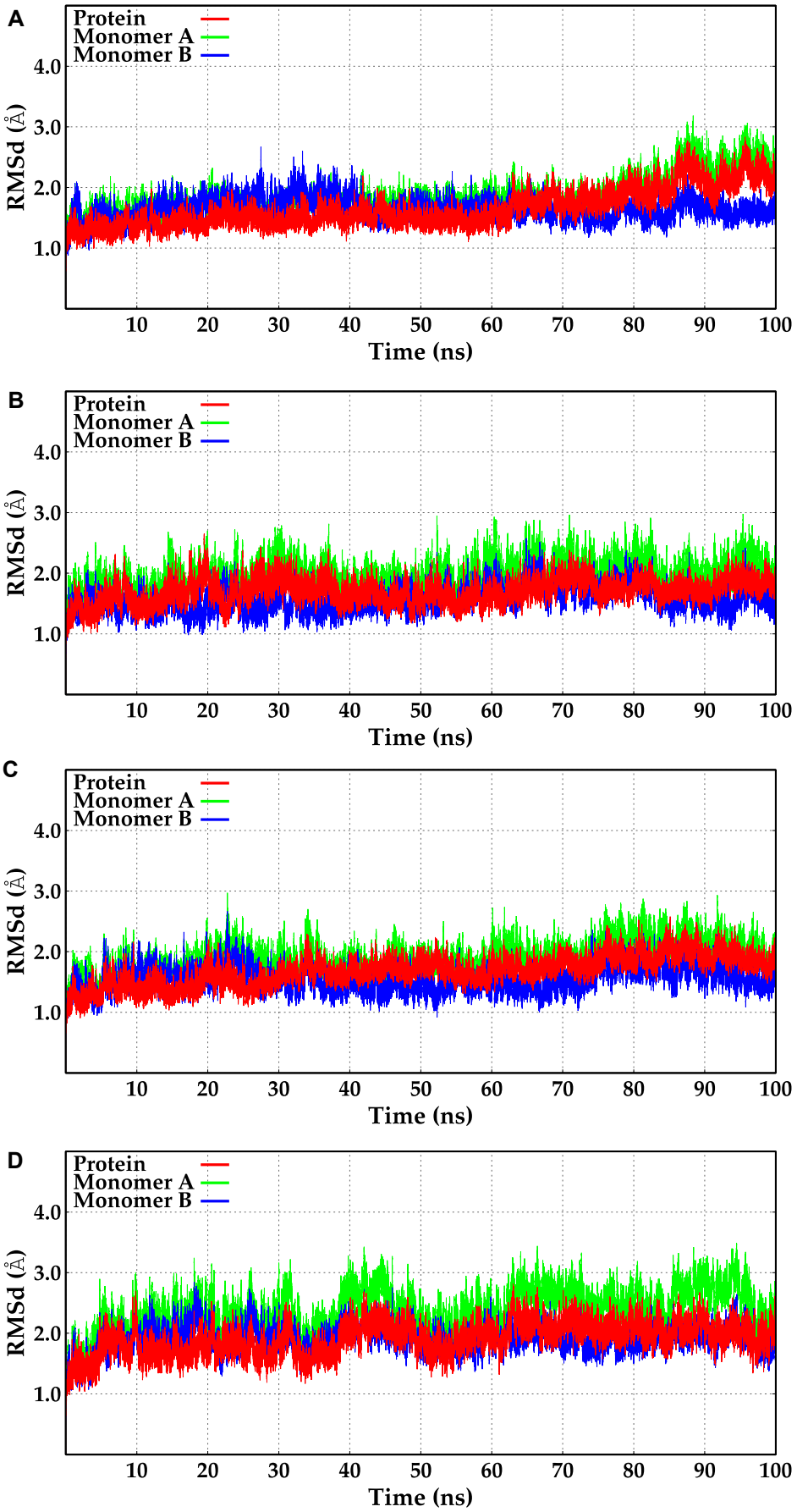

Figure S7. RMSd of backbone atoms (C,C_α,N) along the simulation of (A) T45R variant, (B) T47R variant, (C) S107R variant, and (D) S109R variant.

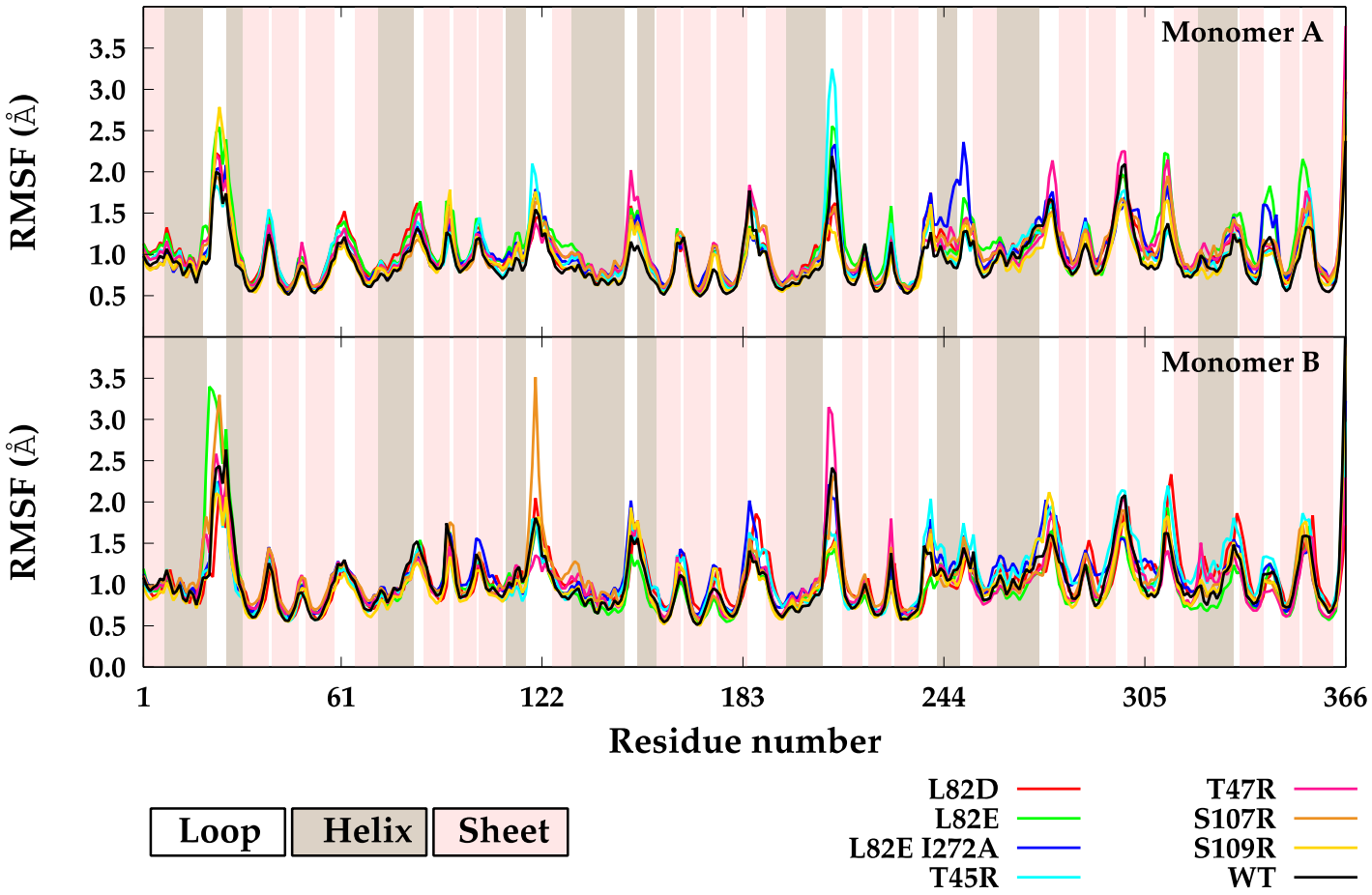

Figure S8. RMSF of residues on Monomer A (top) and Monomer B (bottom) of WT protein (black), L82D variant (red), L82E variant (green), L82E I272A variant (blue), T45R variant (cyan), T47R variant (magenta), S107R variant (orange), and S109R variant (yellow). Residues that are on sheets are represented with light magenta, and the residues that are on helices are represented with light brown columns.

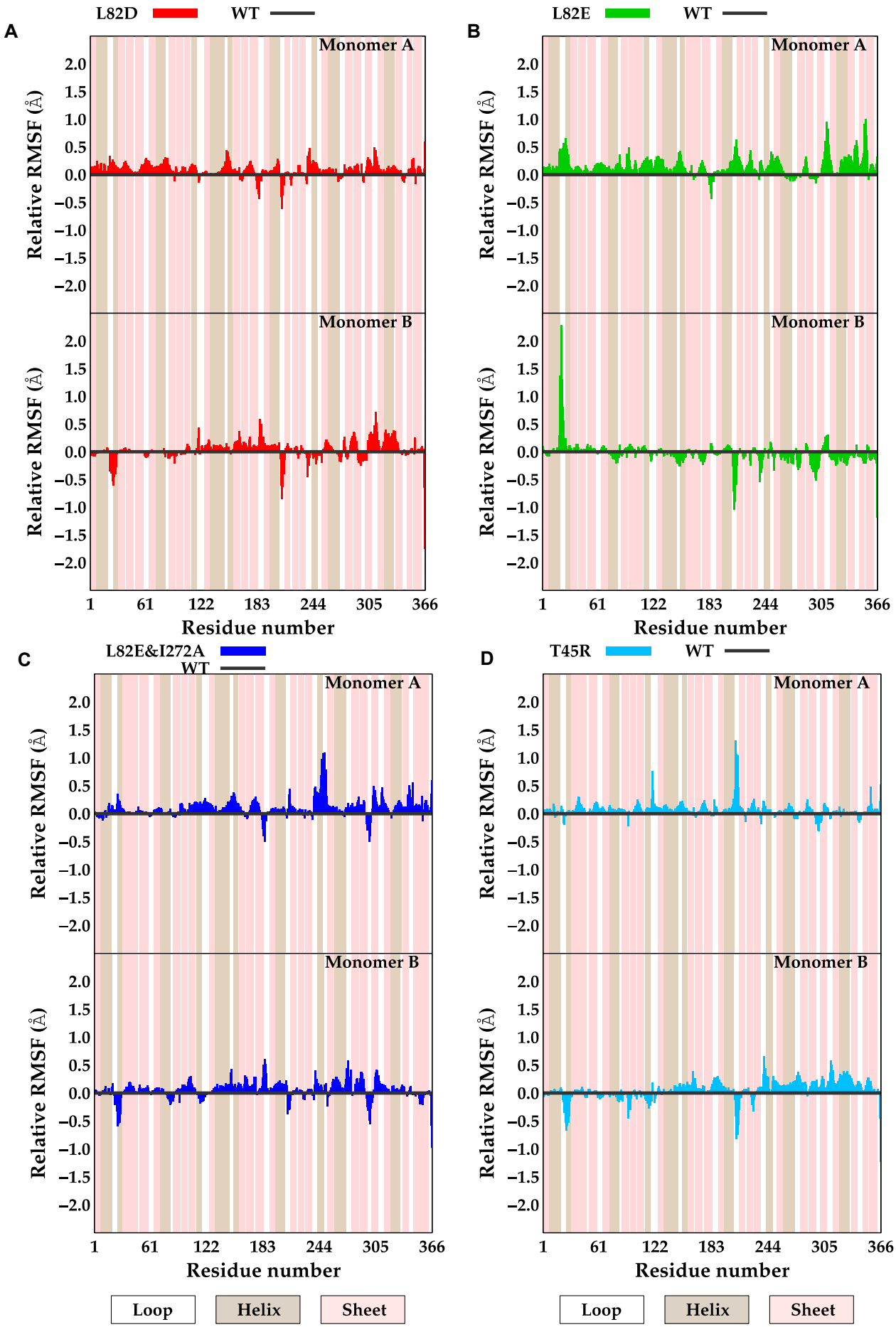

Figure S9. Deviation of the RMSF (Å) values per residue of (A) L82D variant, (B) L82E variant, (C) L82E I272A variant, and (D) T45R variant relative to the WT protein. The relative RMSF values of residues on Monomer A are depicted on top, while the relative RMSF values of residues on Monomer B are depicted on bottom. Residues that are on sheets are represented with light magenta, and the residues that are on helices are represented with light brown columns.

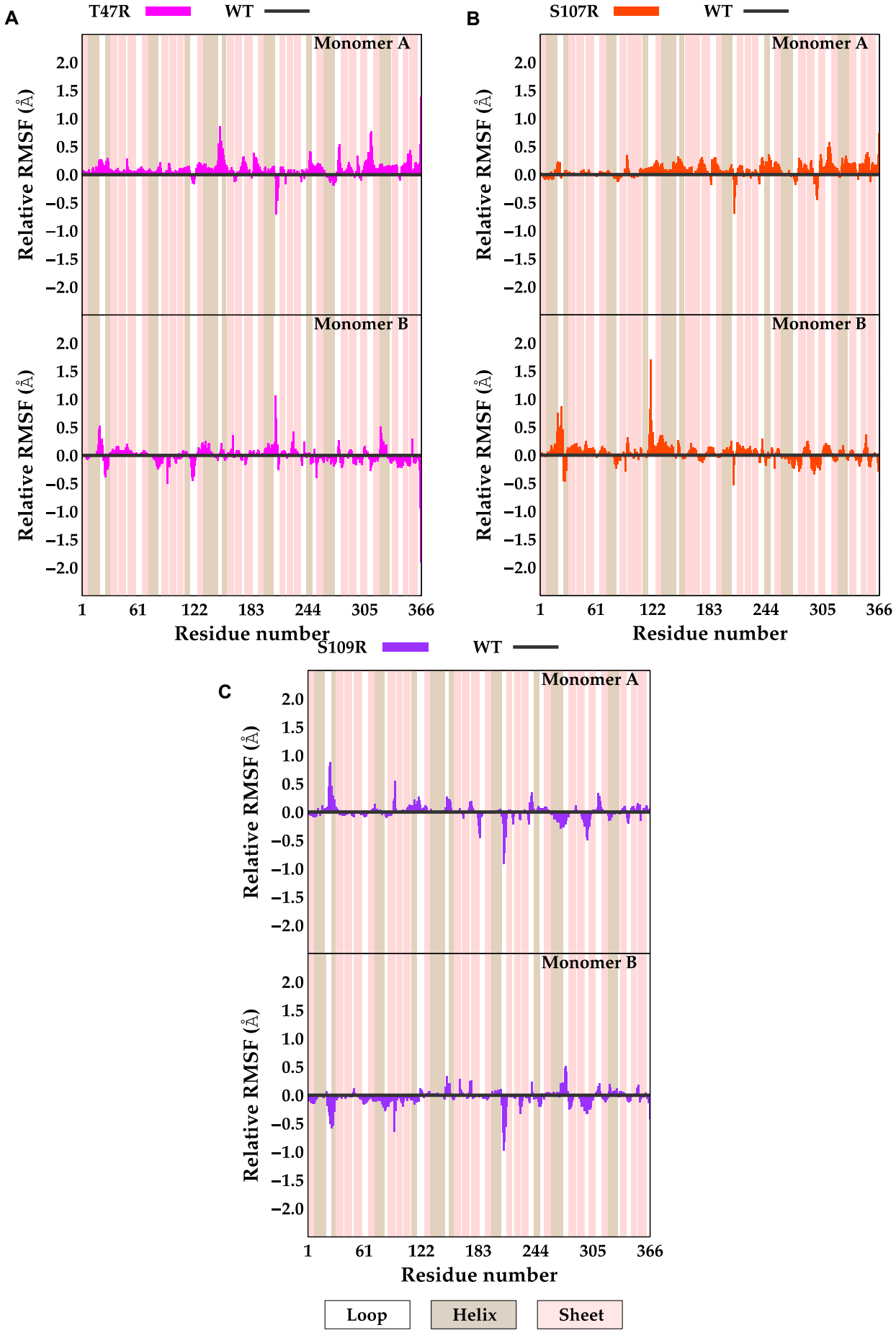

Figure S10. Deviation of the RMSF (Å) values per residue of (A) T47R variant, (B) S107R variant, and (C) S109R variant relative to the WT protein. The relative RMSF values of residues on Monomer A are depicted on top, while the relative RMSF values of residues on Monomer B are depicted on bottom. Residues that are on sheets are represented with light magenta, and the residues that are on helices are represented with light brown columns.

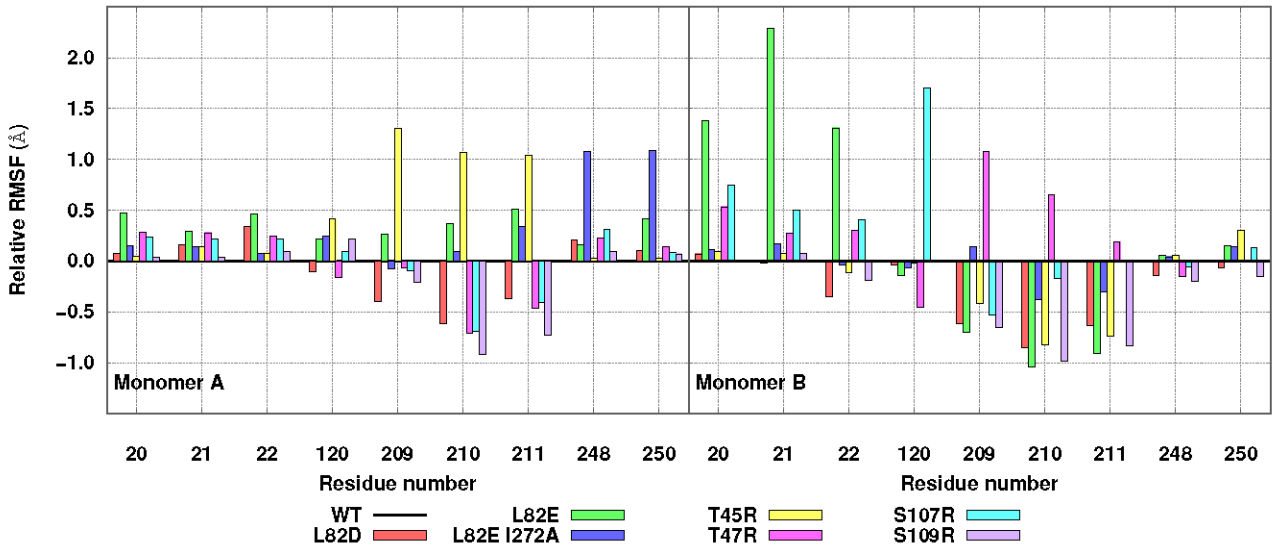

Figure S11. The residues with relative RMSF change greater than 1 Å in at least one monomer. The results for Monomer A are given on the left, and the result for Monomer B are given on the right.

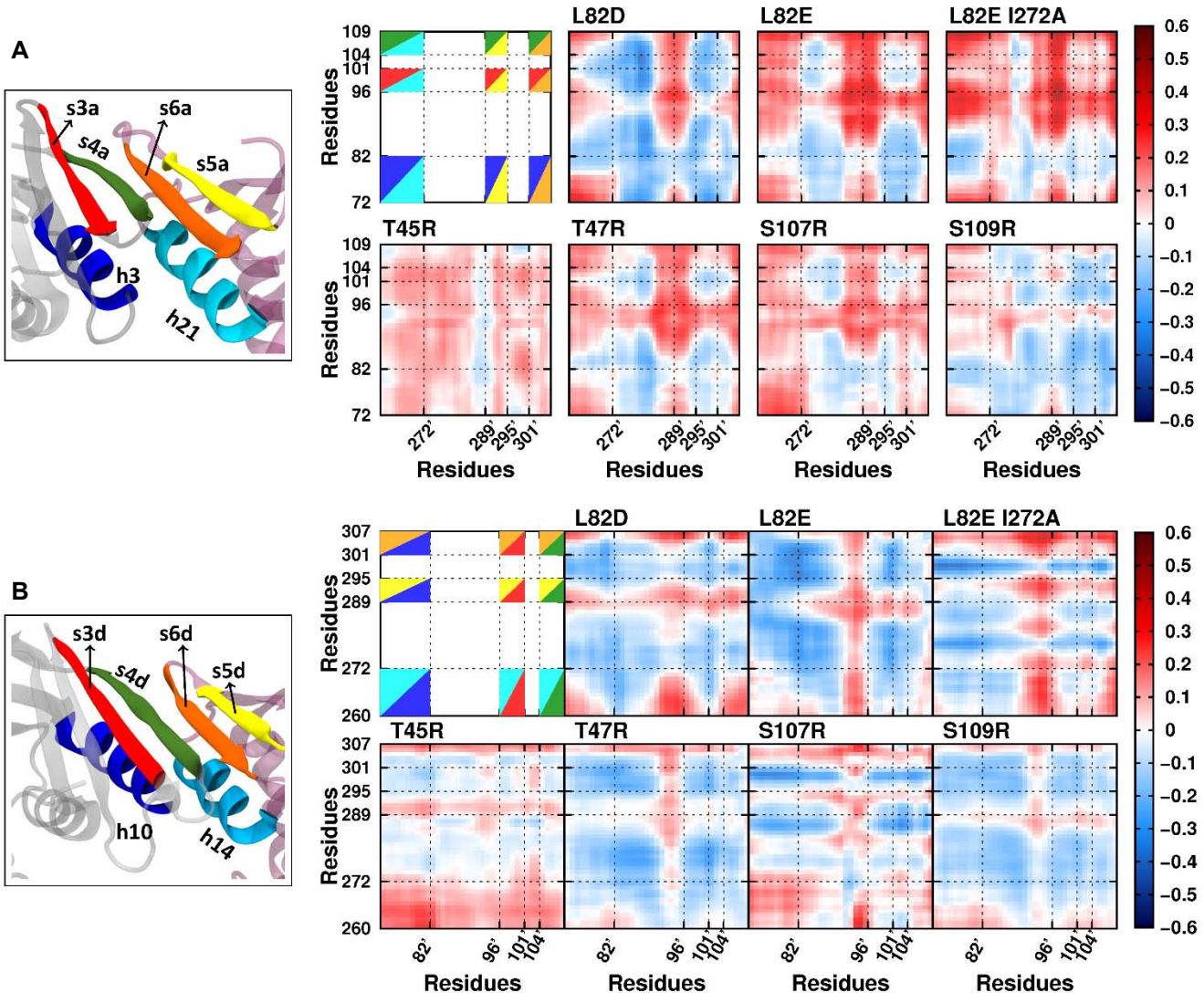

Figure S12. The deviation of the dynamic cross correlations between the residues located on the dimer interfaces of the variants relative to the WT protein. The relative cross correlation between the residues at the (A) dimer interface between Domain 1 and Domain 3', and (B) dimer interface between Domain 3 and Domain 1'. The secondary structures of the residues located at the dimer interfaces are shown on the left in which each secondary structure is depicted with different colors for the corresponding interface. The locations of these secondary structures on the cross-correlation matrices are depicted by the corresponding colors.

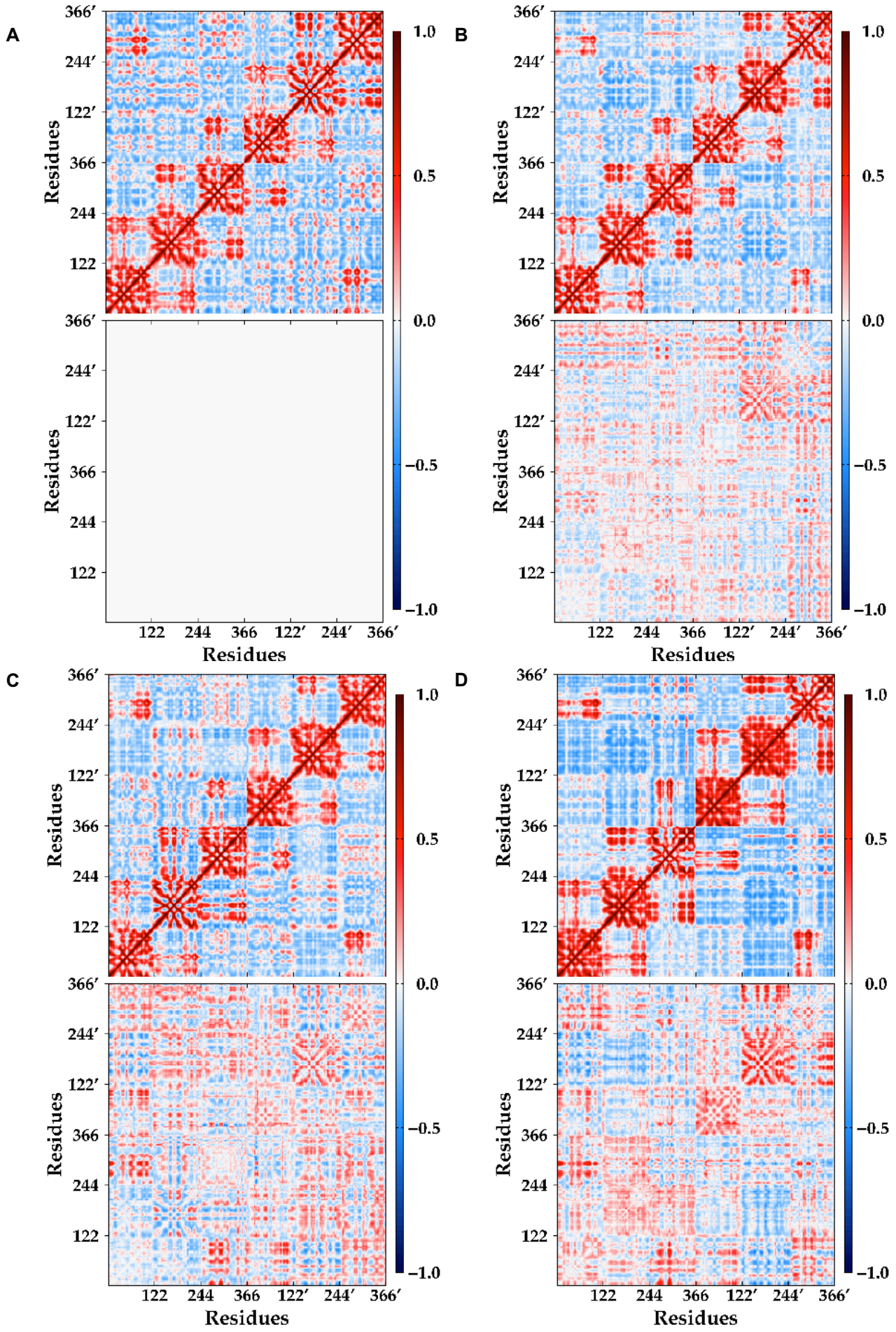

Figure S13. Dynamic cross correlation of the residues of (A) WT protein, (B) L82D variant, (C) L82E variant, and (D) L82E I272A variant. The correlations of the residues are depicted at the top while the deviation of the correlations relative to the reference (WT protein) are given at the bottom.

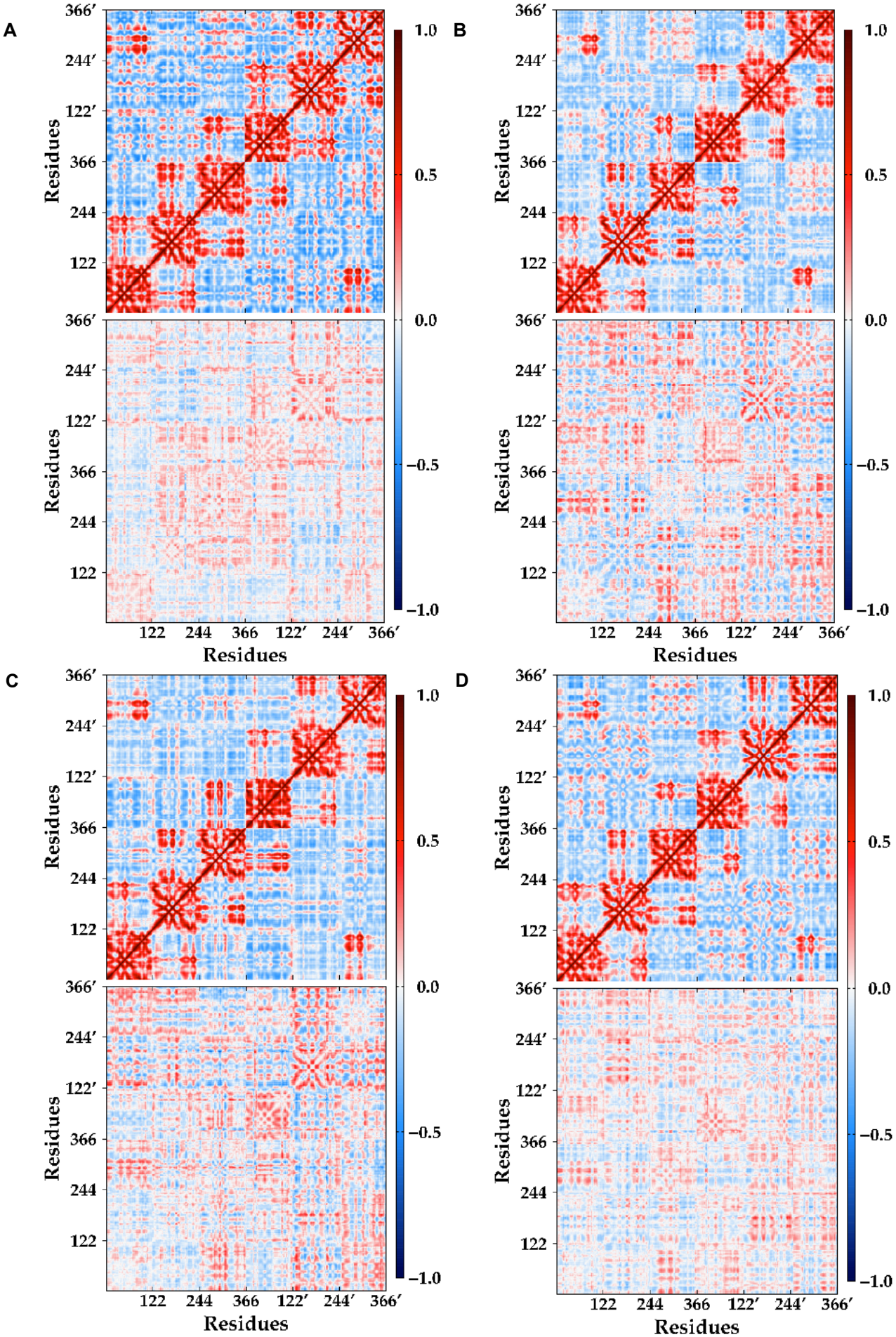

Figure S14. Dynamic cross correlation of the residues of (A) T45R variant, (B) T47R variant, (C) S107R variant, and (D) S109R variant. The correlations of the residues are depicted at the top while the deviation of the correlations relative to the reference (WT protein) are given at the bottom.

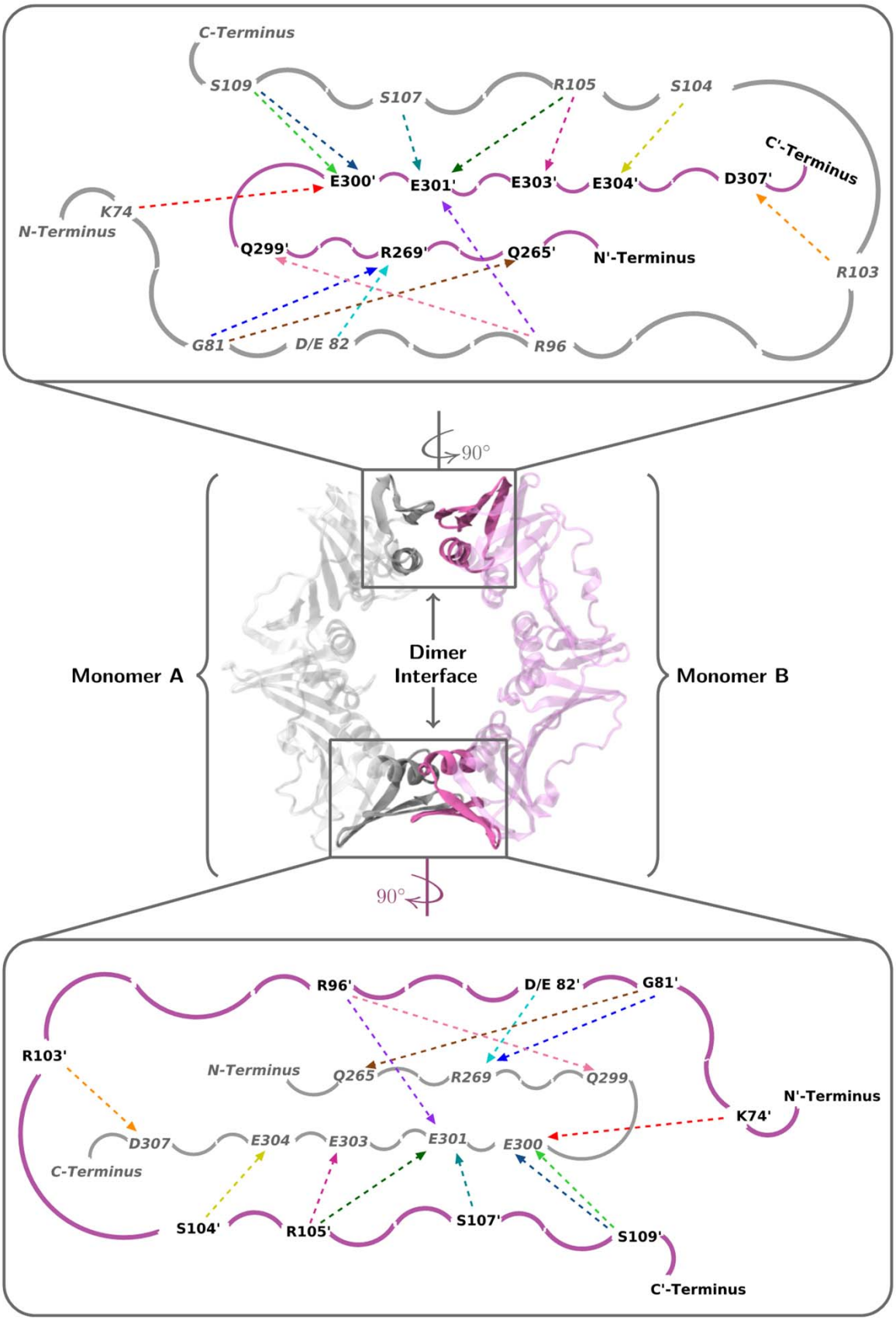

Figure S15. Schematic representation of the hydrogen bond interactions within the dimer interfaces and their locations on the protein. Each of the hydrogen bonds is depicted with a different color. The residues on Monomer A are depicted in gray, while the residues on Monomer B in purple.

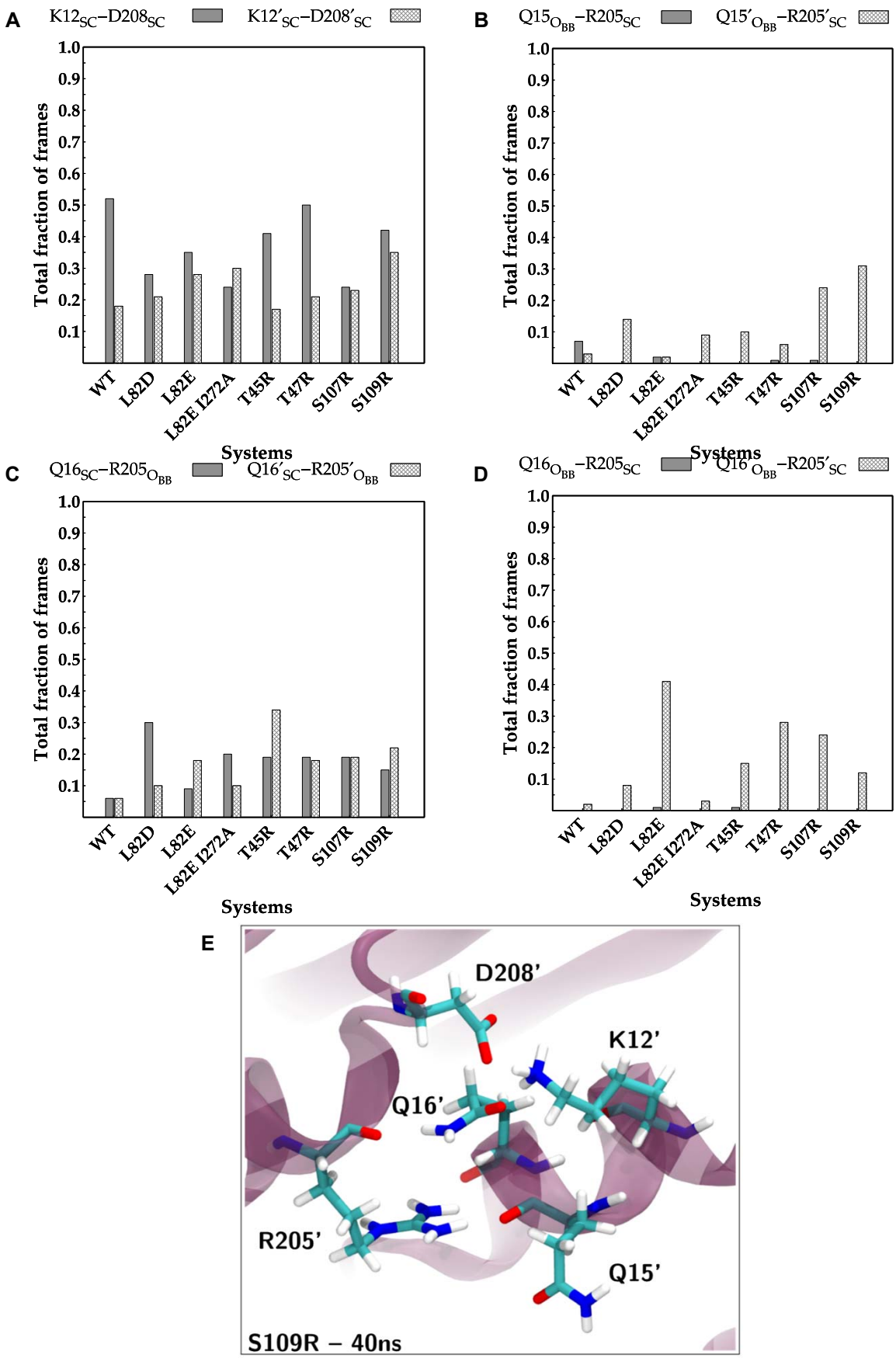

Figure S16. Total fraction of the frames that a hydrogen bond exists between (A) the sidechains of K12 and D208 (solid), and the sidechains of K12' and D208' (pattern fill); (B) the backbone of Q15 and side chain of R205 (solid), and the backbone of Q15' and side chain of R205' (pattern fill); (C) the sidechain of Q16 and backbone of R205 (solid), and the sidechain of Q16' and backbone of R205' (pattern fill); (D) the backbone of Q16 and side chain of R205 (solid), and the backbone of Q16' and side chain of R205' (pattern fill). (E) The three-dimensional representation of the depicted interactions obtained from the trajectory of S109R variant at 40 ns. Sidechains are depicted with subscript "SC" while the backbone Oxygen atoms are depicted with subscript "O_{BB}."

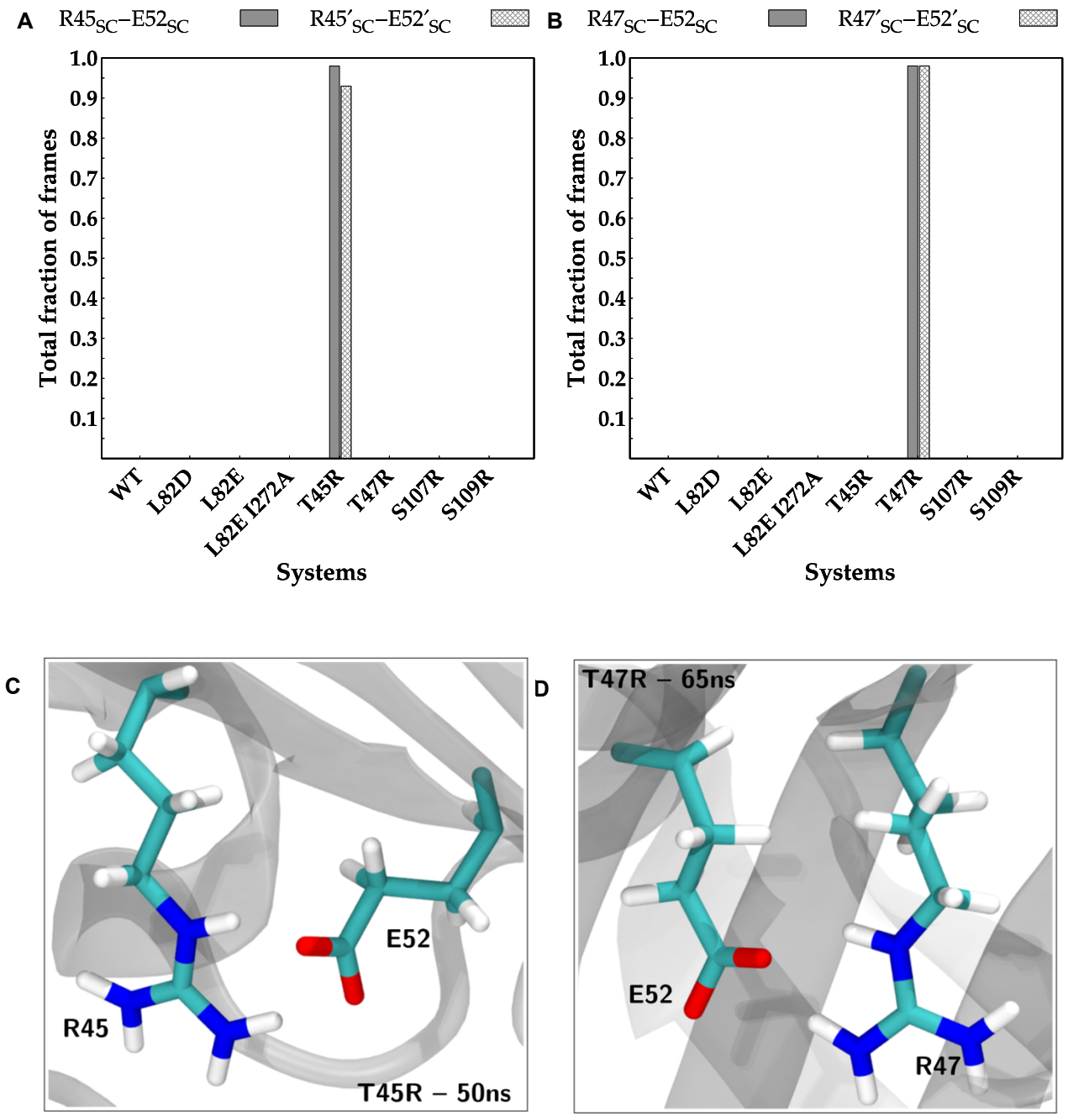

Figure S17. Total fraction of the frames that a hydrogen bond exists between (A) the sidechains of R45 and E52 (solid), and the sidechains of R45' and E52' (pattern fill); (B) the sidechains of R47 and E52 (solid), and the sidechains of R47' and E52' (pattern fill). (C) The three-dimensional representation of the depicted interaction obtained from the trajectory of T45R variant at 50 ns. (D) The three-dimensional representation of the depicted interaction obtained from the trajectory of T47R variant at 65 ns. Sidechains are depicted with subscript "SC."

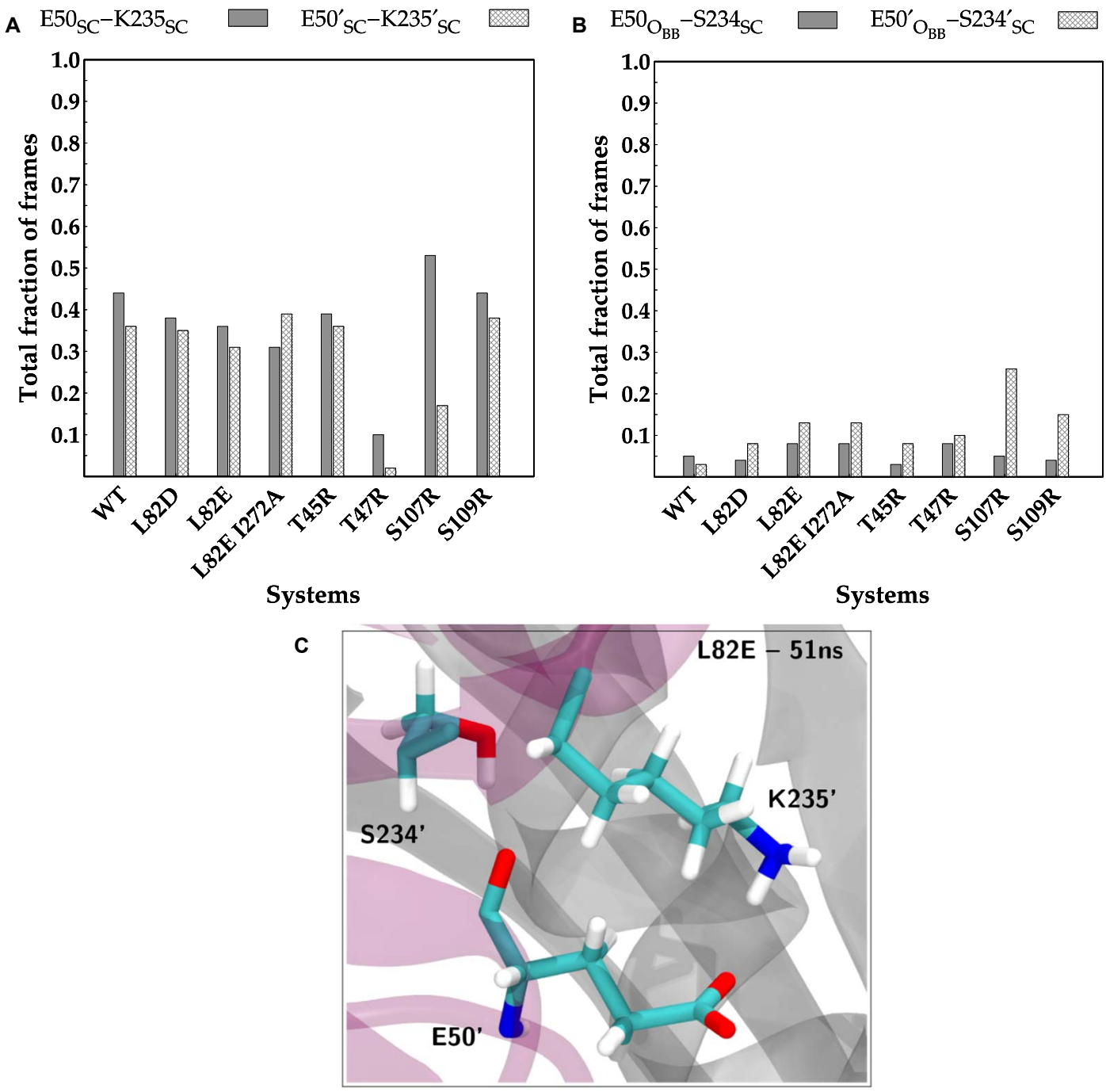

Figure S18. Total fraction of the frames that a hydrogen bond exists between (A) the sidechains of E50 and K235 (solid), and sidechains of E50' and K235' (pattern fill); (B) the backbone of E50 and the sidechain S234 (solid), and the backbone of E50' and the sidechain S234' (pattern fill). (C) The three-dimensional representation of the depicted interaction obtained from the trajectory of L82 variant at 51 ns. Sidechains are depicted with subscript "SC" while the backbone Oxygen atoms are depicted with subscript "O_{BB}."

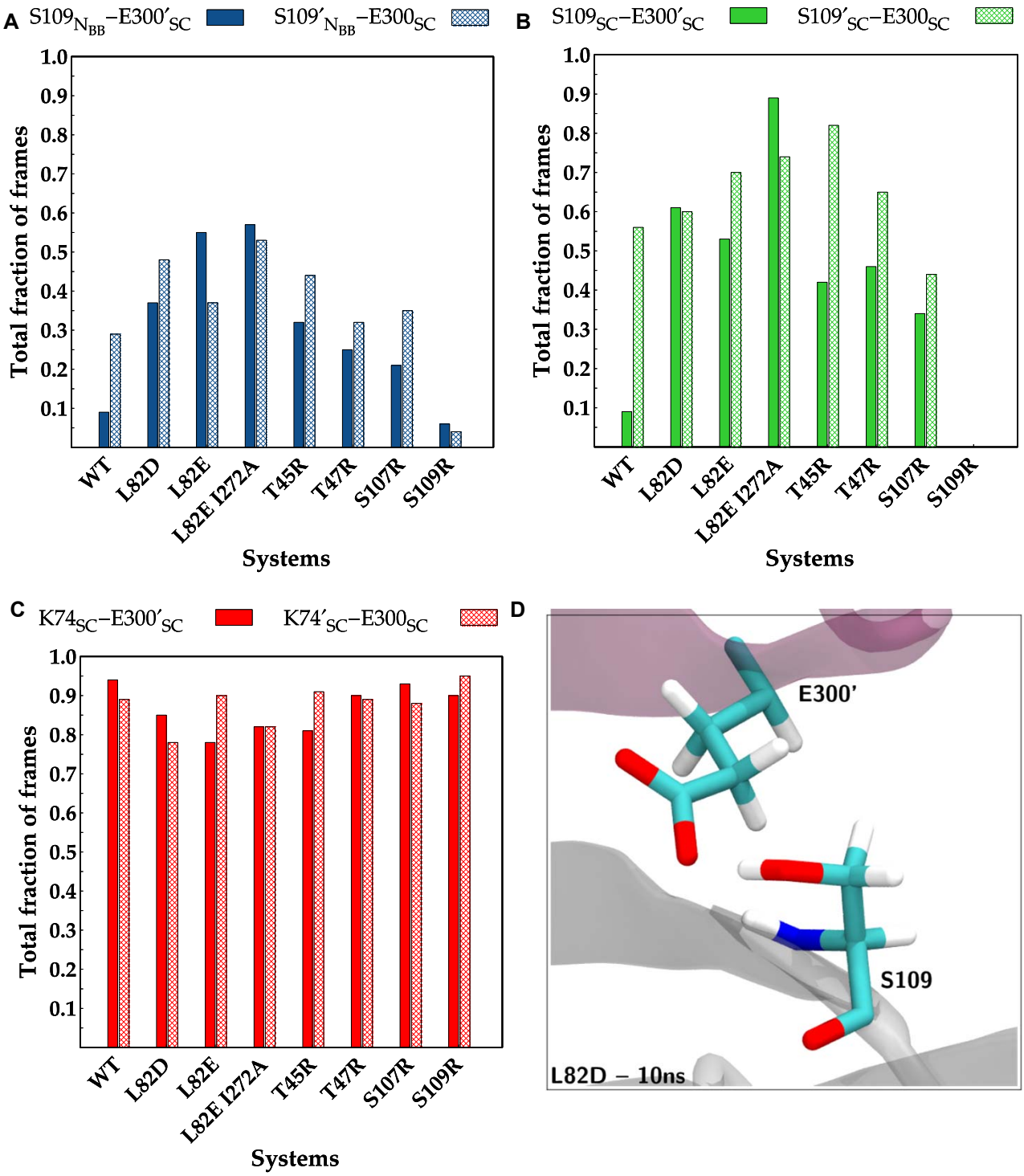

Figure S19. Total fraction of the frames that a hydrogen bond exists between (A) the backbone nitrogen atom of S109 and the sidechain of E300' (solid), and the backbone nitrogen atom of S109' and the sidechain of E300 (pattern fill); (B) the sidechains of S109 and E300' (solid), and sidechains of S109' and E300 (pattern fill); (C) the sidechains of K74 and E300' (solid), and sidechains of K74' and E300 (pattern fill). (D) The three-dimensional representation of the depicted interaction obtained from the trajectory of L82D variant at 10 ns. Sidechain is depicted with subscript "SC" while the backbone Nitrogen atoms are depicted with subscript "N_{BB}."

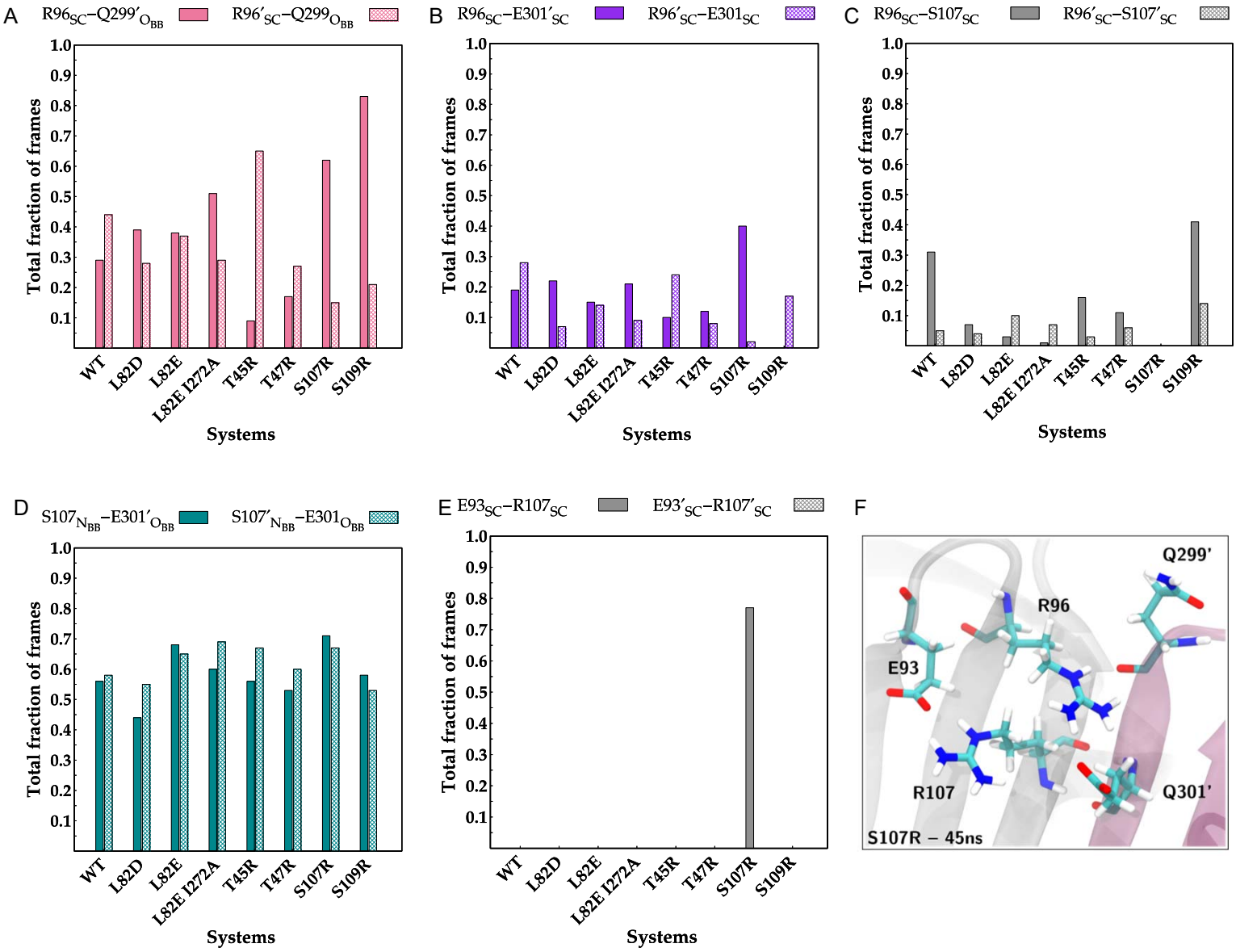

Figure S20. Total fraction of the frames that a hydrogen bond exists between (A) the sidechain of R96 and the backbone oxygen atom of Q299' (solid), and the sidechain of R96' and the backbone oxygen atom of Q299 (pattern fill); (B) the sidechains of R96 and E301' (solid), and the sidechains of R96' and E301 (pattern fill); (C) the sidechains of R96 and S107 (solid), and the sidechains of R96' and S107' (pattern fill); (D) the backbone nitrogen atom of S107 and the backbone oxygen atom of E301' (solid), and the backbone nitrogen atom of S107' and the backbone oxygen atom of E301 (pattern fill); (E) the sidechains of E93 and R107 (solid), and the sidechains of E93' and R107' (pattern fill). (F) The three-dimensional representation of the depicted interaction obtained from the trajectory of S107R variant at 45 ns. Sidechains are depicted with subscript "SC" while Nitrogen and Oxygen atoms on the backbone are depicted with subscripts "N_{BB}" and "O_{BB}," respectively.

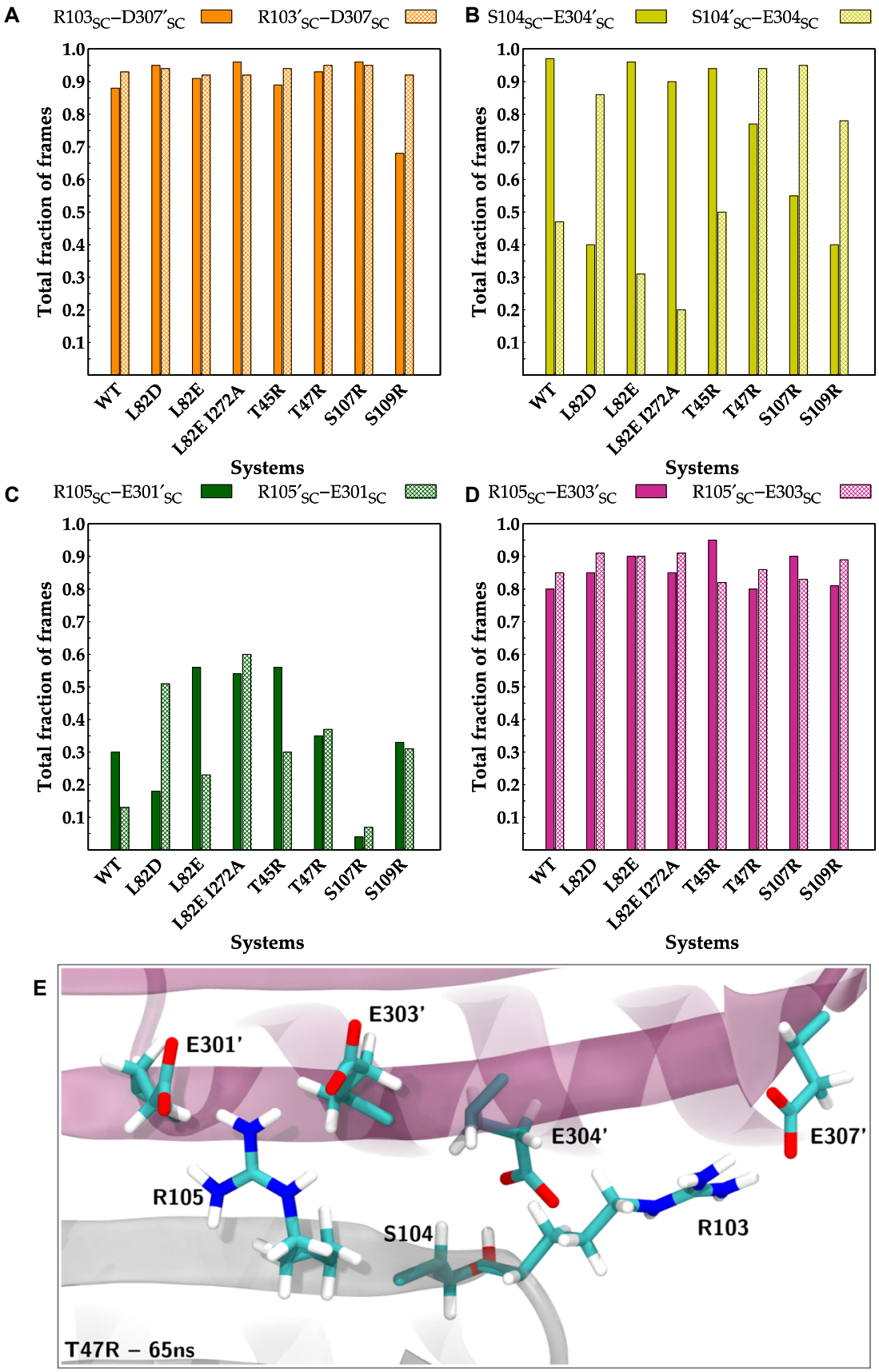

Figure S21. Total fraction of the frames that a hydrogen bond exists between (A) the sidechains of R103 and D307' (solid), and the sidechains of R103' and D307 (pattern fill); (B) the sidechains of S104 and E304' (solid), and the sidechains of S104' and E304 (pattern fill); (C) the sidechains of R105 and E301' (solid), and the sidechains of R105' and E301 (pattern fill). (D) the sidechains of R105 and E303' (solid), and the sidechains of R105' and E303 (pattern fill). (E) The three-dimensional representation of the depicted interactions obtained from the trajectory of T47R variant at 65 ns. Sidechains are depicted with subscript "SC."